Supporting Information for

Supported Molecular Iridium Catalysts: Resolving Effects of Metal Nuclearity and Supports as Ligands

Jing Lu,[1] Pedro Serna,[1] Ceren Aydin,[1] Nigel D. Browning,[1,2] Bruce C. Gates[1*]

[1]Department of Chemical Engineering and Materials Science, University of California-Davis, One Shields Avenue, Davis, California 95616, USA

[2]Physical and Life Sciences Directorate, Lawrence Livermore National Laboratory, 7000 East Avenue, Livermore, California 94550, USA

[*] E-mail address: bcgates@ucdavis.edu

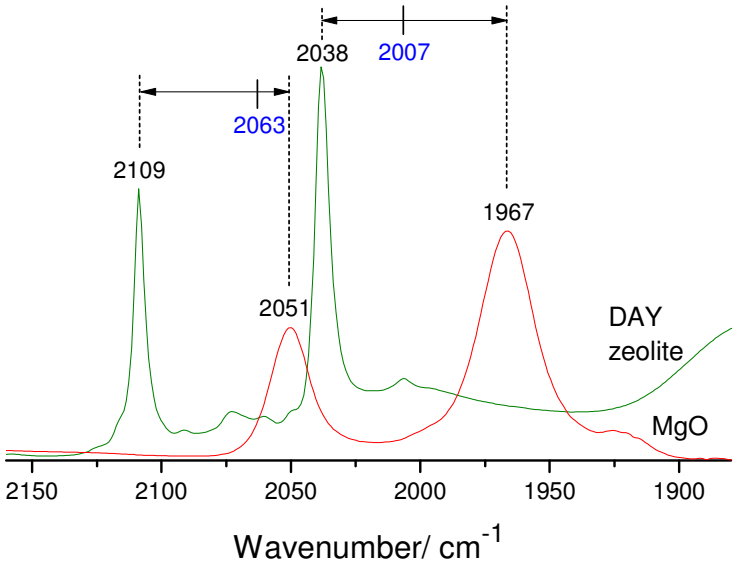

Figure S1. IR spectra characterizing the samples formed by adsorption of $Ir(C_2H_4)_2(acac)$ on highly dehydroxylated MgO and dealuminated HY zeolite (DAY zeolite) after probing of the supported species with CO flowing at 298 K and 1 bar for 30 s. The two pairs of bands indicate the formation of iridium *gem*-dicarbonyl species. The sharpness of the bands indicates that the structures of the iridium sites have a relatively high degree of uniformity on each support, although the sharper bands characterizing the zeolite-supported sample show that the local structure is more uniform on the zeolite than on the MgO, with the iridium complexes bonding to the zeolite surface specifically at Al^{3+} sites, as shown by EXAFS spectroscopy. The positions of the dicarbonyl bands indicate the character of MgO as an electron-donating ligand and of DAY zeolite as an electron-withdrawing ligand (the back-donation of filled d-metal orbitals into π^*-antibonding orbitals of CO is favored when the metal is electron-enriched on MgO, which causes a shift of the ν_{CO} stretching frequency to lower wavenumbers compared with the $Ir(CO)_2(acac)$ precursor, 2007 and 2063 cm^{-1}, and vice versa for DAY zeolite). This figure is also presented in the text, but with fewer details than are given here.

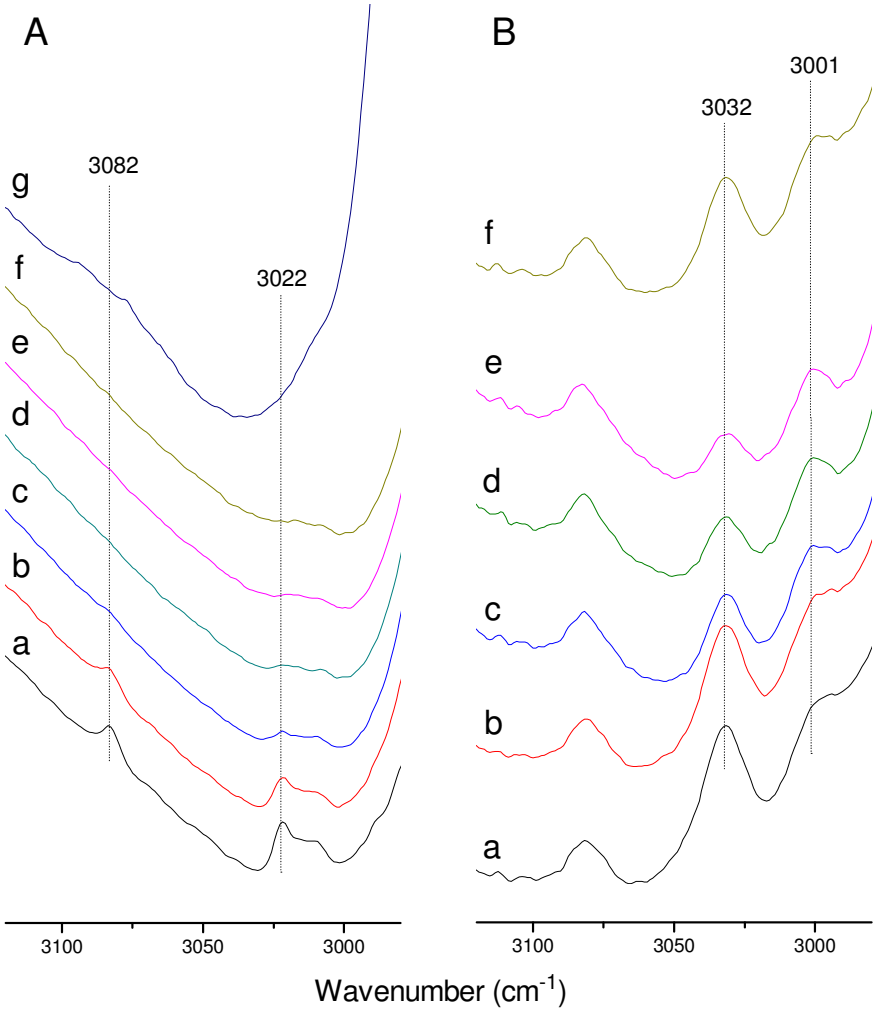

Figure S2. IR spectra in the ν_{CH} region characterizing (A) DAY zeolite-supported $Ir(C_2H_4)_2$ complexes treated in flowing gases at 298 K and atmospheric pressure in the following sequence: helium followed by H_2 for the following times (min): (a) 0, (b) 2, (c) 4, (d) 6, (e) 8, (f) 10, and (g) helium followed by ethene + H_2 (with ethene hydrogenation catalysis) for 10 min (spectrum recorded after purging of gas phase C_2H_4 and H_2 with helium). (B) MgO-supported $Ir(C_2H_4)_2$ similarly treated at 298 K and atmospheric pressure in the following sequence: helium followed by H_2 for the following times (min): (a) 0, (b) 10, (c) 60, (d) 120, (e) 180, and (f) helium followed by ethene + H_2 (with ethene hydrogenation catalysis) for 10 min (spectrum recorded after purging of gas phase C_2H_4 and H_2 with helium). This figure is also presented in the text, but with fewer details than are given here.

In the continuous flow of H_2 at 298 K, the disappearance of the bands ascribed to ethene ligands initially π-bonded to mononuclear iridium species (3022 and 3082 cm^{-1} when the support was DAY zeolite and 3001 and 3032 cm^{-1} when the support was MgO) took place rapidly on the zeolite-supported sample, whereas it took place very slowly on MgO-supported sample. After feeding mixtures of H_2 + C_2H_4 (for several turnovers of the catalytic reaction), the virtual

absence of bands at 3022 and 3082 cm^{-1} shows that ethene was essentially no longer π-bonded to the iridium, in contrast to the result observed for the MgO-supported sample.

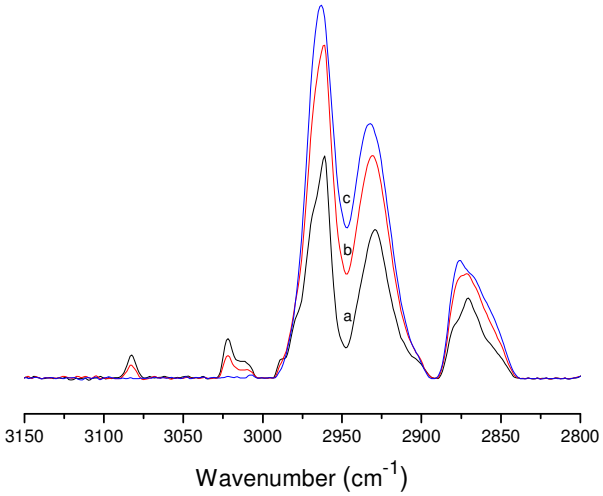

Figure S3. Baseline-corrected IR spectra in the ν_{CH} region characterizing DAY zeolite-supported $Ir(C_2H_4)_2$ treated in flowing H_2 at 298 K for the following times (min): (a) 0 (black line), (b) 2 (red line), and (c) 4 (blue line).

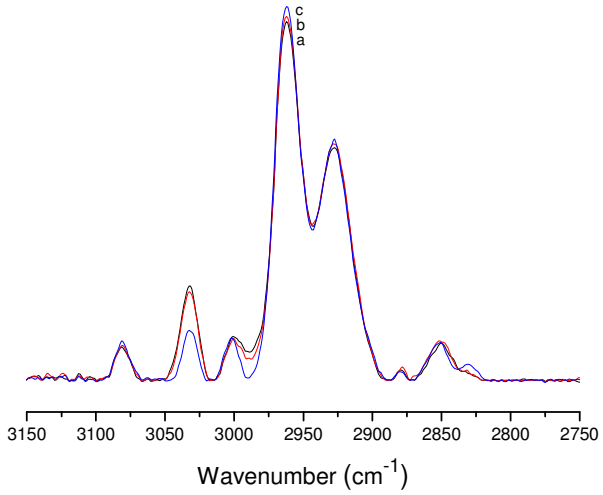

Figure S4. Baseline-corrected IR spectra in the ν_{CH} region characterizing MgO-supported $Ir(C_2H_4)_2$ treated in flowing H_2 at 298 K for the following times (min): (a) 0 (black line), (b) 10 (red line), and (c) 120 (blue line).

The results of time-resolved IR experiments carried out with the samples in flowing H_2 at 298 K and 1 bar show that the reaction of the iridium complexes with H_2 led to the conversion of the ligands initially bonded to the Ir atoms to form ethyl ligands, evidenced by a decrease in the intensity of the bands at 3001 and 3032 cm^{-1}, when the support was MgO, and those at 3022 and 3088 cm^{-1}, when the support was DAY zeolite, assigned to C–H stretching vibrations of ethene bonded to the single Ir atoms, with the concomitant growth of new bands at 2964, 2936, 2876, and 2854 cm^{-1} (for the zeolite-supported sample), and 2963, 2930, and 2829 cm^{-1} (for the MgO-supported sample), related to formation of ethyl ligands;[1] this process was fast on the zeolite-

supported sample (a complete disappearance of the ethene ligands occurred within the first 5 min of the treatment) but slow on MgO (a minor disappearance of these ligands was observed after 2 h of treatment).

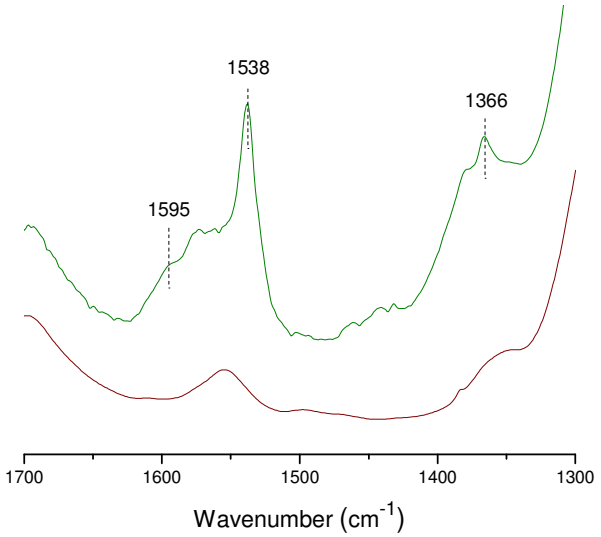

Figure S5. IR spectra in the region of 1200–1700 cm^{-1} characterizing a blank sample (DAY zeolite) after calcination at 773 K (bottom) and the sample formed by reaction of calcined DAY zeolite with $Ir(C_2H_4)_2(acac)$ in *n*-pentane (the spectrum was recorded after removal of the solvent) (top). The peaks at 1366, 1538, and 1595 cm^{-1} are assigned to δ_{CH}, $\nu_{C–C–Cs}$, and ν_{COring} of Hacac adsorbed on DAY zeolite. The data indicate the dissociation of the acac ligand from Ir atoms in the chemisorption of the precursor.[2]

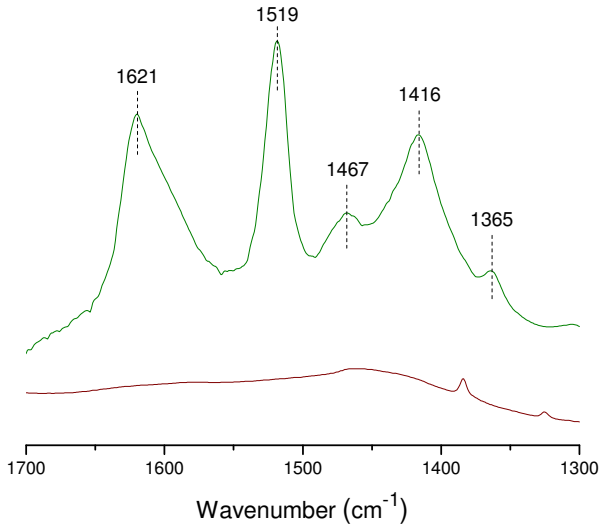

Figure S6. IR spectra in the region of 1200–1700 cm^{-1} characterizing a blank MgO sample after calcination at 973 K (bottom) and the sample formed by reaction of calcined MgO with $Ir(C_2H_4)_2(acac)$ in *n*-pentane (the spectrum was recorded after removal of the solvent) (top). The peaks at 1365, 1416, 1467, 1519, and 1621 cm^{-1} are assigned to δ_{CH}, $\nu_{C–C–Cs}$, and ν_{COring} of Hacac adsorbed on MgO. The data indicate the dissociation of the acac ligand from the Ir atoms during the chemisorption of the precursor.[3]

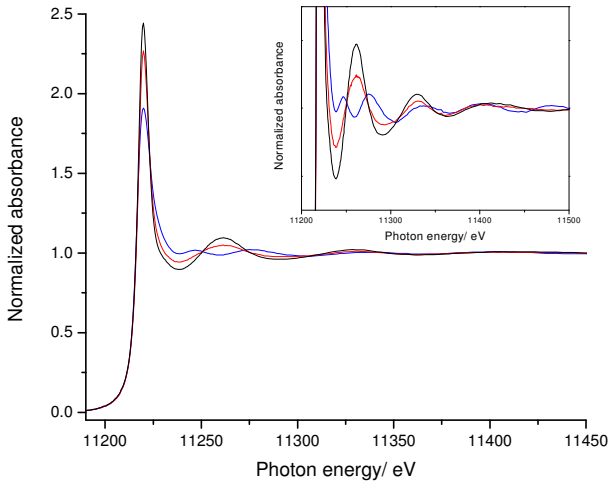

Figure S7. XANES spectra at the Ir L_{III}-edge characterizing the DAY zeolite-supported iridium species under the following treatment conditions: $Ir(C_2H_4)_2$ in flowing helium (black line), $Ir(C_2H_4)_2$ in a continuous stream of C_2H_4 and H_2 (with ethene hydrogenation catalysis occurring) at 298 K and atmospheric pressure for 2 h (red line), $Ir(C_2H_4)_2$ in a continuous stream of H_2 at 353 K and atmospheric pressure for 1 h (blue line).

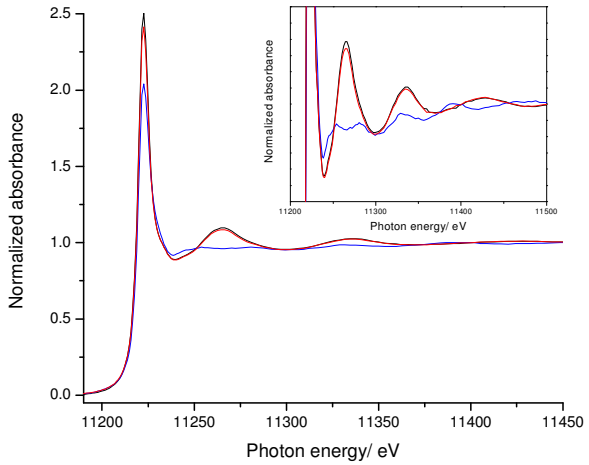

Figure S8. XANES spectra at the Ir L_{III}-edge characterizing the MgO-supported iridium species under the following treatment conditions: $Ir(C_2H_4)_2$ in flowing helium (black line), $Ir(C_2H_4)_2$ in a continuous stream of C_2H_4 and H_2 (with ethene hydrogenation catalysis occurring) at 298 K and atmospheric pressure for 2 h (red line), $Ir(C_2H_4)_2$ in a continuous stream of H_2 at 353 K and atmospheric pressure for 1 h (blue line).

The X-ray absorption near edge structure (XANES) spectra, which are sensitive to subtle changes in the chemical environment of the iridium species, show that the intensity of the white line corresponding to the initially prepared iridium complexes decreased in intensity after the complexes had been converted into clusters at 353 K, but the change was much less significant when the samples were treated in the H_2-rich stream at 298 K (the white line intensity is related to the transition of core electrons to unoccupied d-electron orbitals). The formation of clusters from mononuclear species usually leads to a significant decrease of the white line intensity, as the d-electron orbitals are further filled as a result of the new metal-metal bonds. This observation, and the fact that the XANES signature characterizing the catalyst after operation at

298 K is markedly different from that characterizing the supported iridium clusters, are consistent with the inference that the iridium species remained mononuclear during the catalysis, undergoing only changes in the ligands as a result of contact with the reactive H_2 + C_2H_4 mixture, was also indicated by the EXAFS data—these subtle changes are support-dependent.

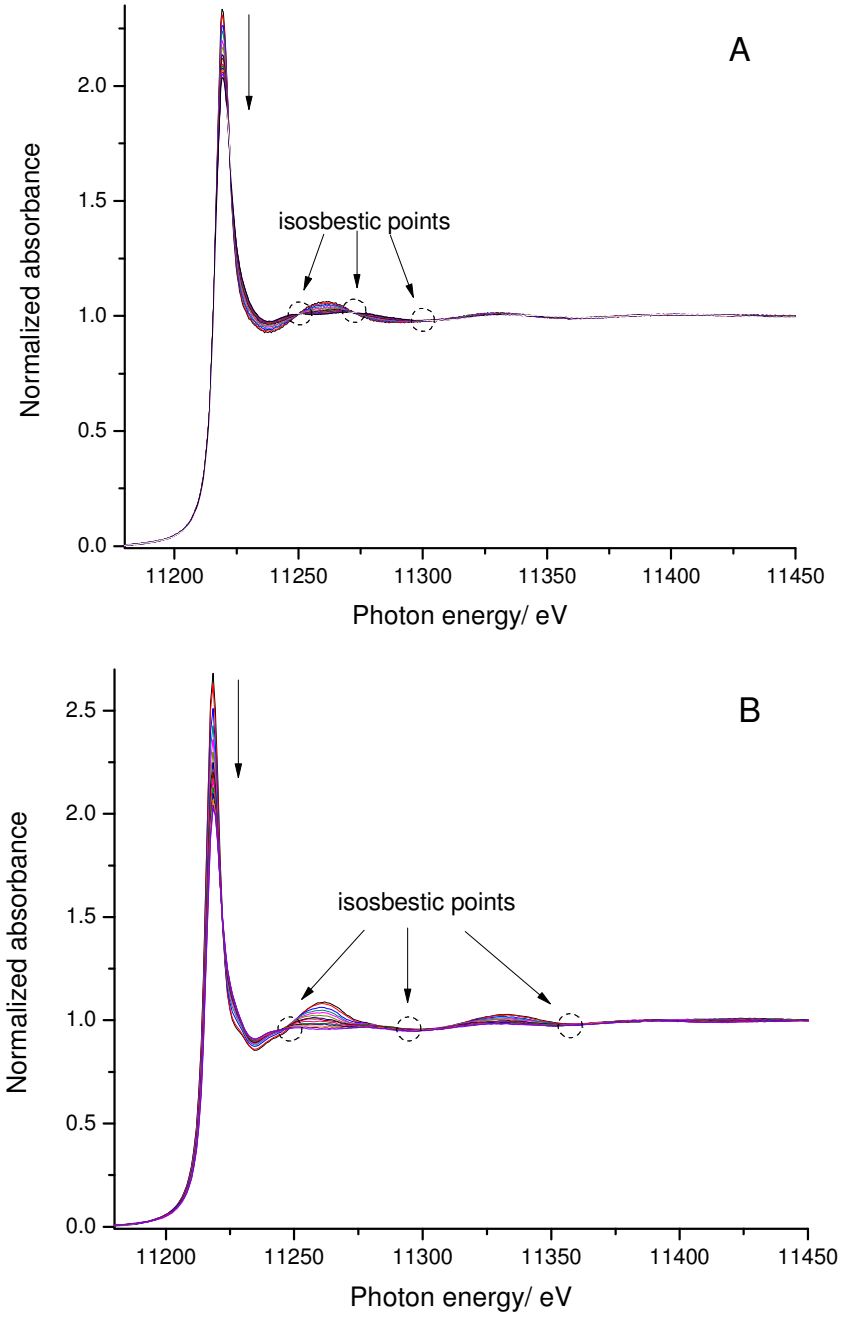

Figure S9. Normalized XANES spectra at the Ir L_{III} edge characterizing the sample formed by the chemisorption $Ir(C_2H_4)_2(acac)$ on (A) DAY zeolite and (B) MgO; spectra were recorded during the cluster formation at 353 K with the samples in flowing H_2 for 1 h at atmospheric pressure. The isosbestic points indicate the almost stoichiometric conversion of one species to another. The decrease of the white line intensity indicates the reduction of the initially mononuclear iridium species (i.e., cluster formation).

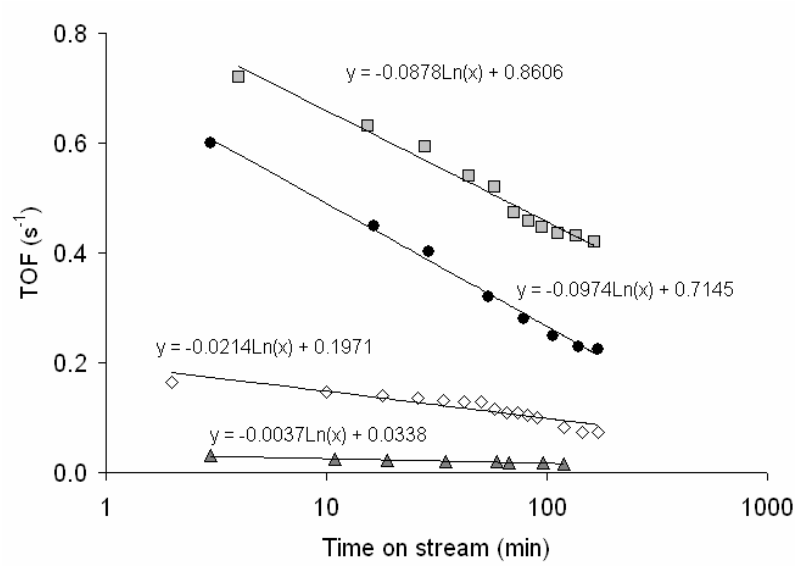

Figure S10. Evolution of the catalytic activity of MgO- and DAY zeolite-supported mononuclear iridium complexes and iridium clusters (approximated as Ir_4) for the hydrogenation of ethene as a function of time on stream in the flow reactor in the presence of H_2 at 303 K and 1 bar (0.2 mbar of C_2H_4, 0.4 mbar of H_2; the balance was helium). The data show a deactivation of the catalyst reflecting changes in the ligand environment of the metal. Symbols: □ clusters approximated as tetrairidium supported on DAY zeolite; ● mononuclear iridium complexes supported on DAY zeolite; ◇ tetrairidium clusters supported on MgO; △ mononuclear iridium complexes supported on MgO.

Table S1: Summary of EXAFS fit parameters characterizing the dealuminated Zeolite Y-supported iridium Complex after various treatments.

		N	*R*(Å)	$10^3 \times \Delta\sigma^2$ (Å^2)	ΔE_0(eV)	*k*-range		*R*-range		Error in EXAFS function[b]	Goodness of fit[c]
As prepared sample	Ir-$O_{support}$	2.0	2.10	0.6	-5.9	3.81	12.50	0.5	3.8	0.0009	1.5
	Ir-C	3.9	2.03	9.0	0.26						
	Ir-Al	1.0	2.97	8.5	-8.0						
	Ir-O_{long}	1.5	3.50	4.8	5.0						
After 2 h of ethene hydrogenation reaction at 298 K	Ir-$O_{support}$	2.2	2.13	3.5	-6.3	3.81	13.74	0.5	3.8	0.0013	2.9
	Ir-C	2.1	1.98	6.6	7.5						
	Ir-Al	1.0	2.95	4.1	-5.9						
	Ir-C_{long}	1.9	3.20	1.1	8.0						
After 20 min in H_2 flow at 298 K	Ir-$O_{support}$	1.9	2.11	7.2	-2.6	3.79	12.05	0.5	3.8	0.005	4.3
	Ir-C	1.8	2.02	10	-2.7						
	Ir-Al	1.1	2.98	5.4	-8.0						
	Ir-C_{long}	1.7	3.20	5.0	0.20						
After 1 h in H_2 flow at 353 K	Ir-$O_{support}$	0.80	2.10	2.9	8.0	3.03	13.51	0.5	3.8	0.0006	9.5
	Ir-C	1.6	2.00	14	8.0						
	Ir-Al	0.89	2.91	0.3	1.7						
	Ir-Ir	3.1	2.67	7.9	-4.1						

[a] Notation: $O_{support}$, oxygen from support; O_{long}, oxygen from support in a distance longer than bonding distance; C_{long}, carbon from an ethyl group that is not directly bonded to the metal; *N*, coordination number; *R*, distance between absorber and backscatterer atoms; $\Delta\sigma^2$, Debye-Waller factor; ΔE_0, Inner potential correction. Error bounds (accuracies) characterizing the structural parameters, obtained by EXAFS spectroscopy are estimated to be as follows: *N*, ± 20%; *R*, ± 0.02Å; $\Delta\sigma^2$, ± 20%; and ΔE_0, ± 20%. [b] The error in the data was calculated as the root mean square of the value obtained from the subtraction of smoothed χ data from the background-subtracted experimental χ values. [c] Goodness of fit values were calculated with the software XDAP, as follows: $goodness\ of\ fit = \frac{\nu}{NPTS\left(\nu - N_{free}\right)} \sum_{i=1}^{NPTS} \left(\frac{\chi_{\exp,i} - \chi_{\mathrm{model},i}}{\sigma_{\exp,i}} \right)^2$ The terms χ_{model} and χ_{exp} are the model and experimental EXAFS values, respectively; σ_{exp} is the error in the experimental results; ν is the number of independent data points in the fit range; and NPTS is the actual number of data points in the fit range; N_{free} is the number of free parameters. [d] Number of statistically justified parameters was calculated by using the Nyquist theorem, as follows: number of justified parameters = $n = (2\Delta k \Delta R/\pi) + 2$, where Δk and ΔR are the *k*- and *R*- ranges used the fitting.

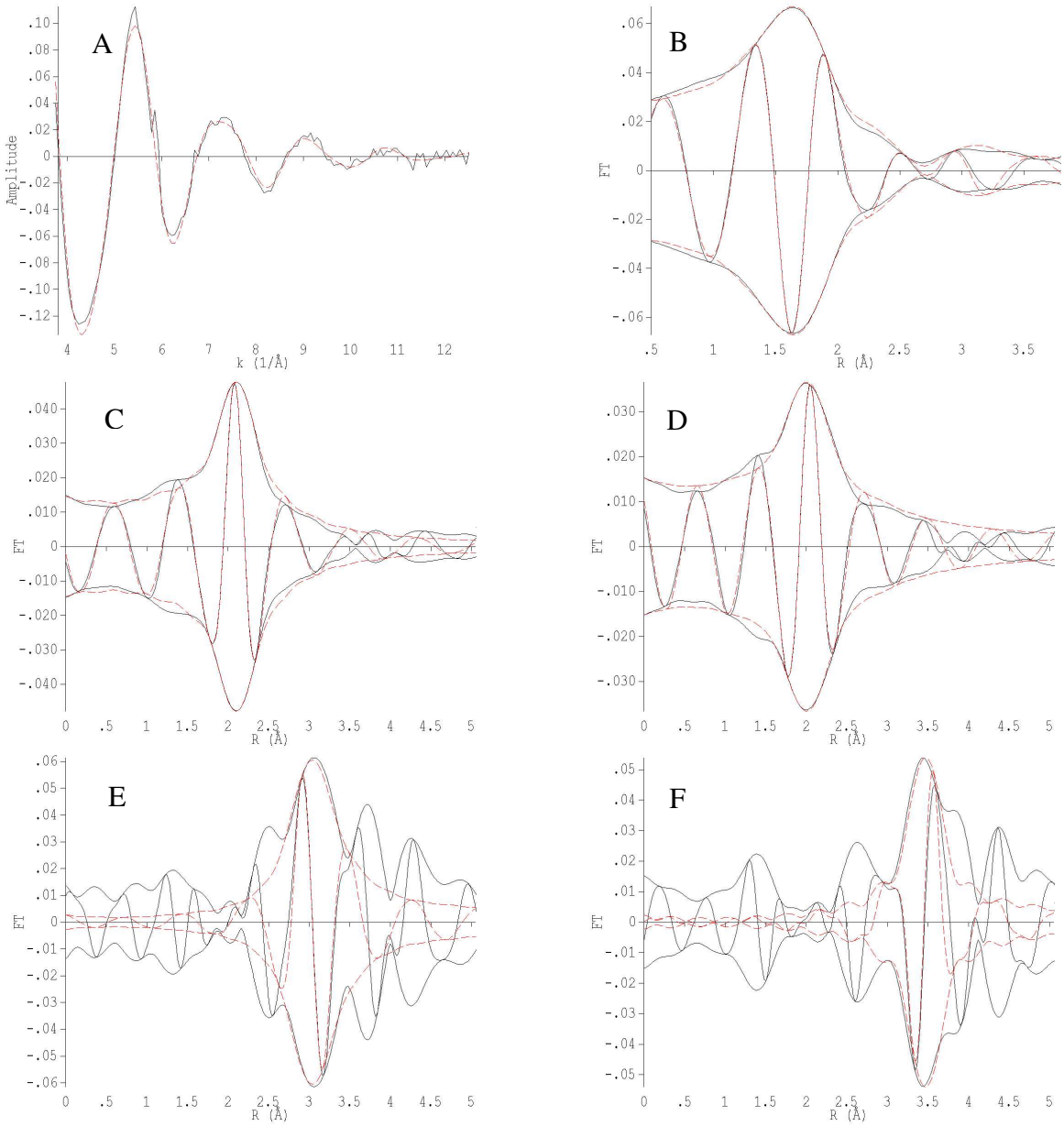

Figure S11. EXAFS data characterizing initially prepared highly dealuminated zeolite Y-supported iridium complex formed by adsorption of $Ir(C_2H_4)_2(acac)$ on the zeolite: (A) k^1-weighted EXAFS function, $k^1(\chi)$ (solid line) and sum of the calculated contributions (dashed line); (B) k^1-weighted imaginary part and magnitude of the Fourier transform of the data (solid line) and sum of the calculated contributions (dashed line); (C) k^1-weighted, phase-corrected, imaginary part and magnitude of the Fourier transform of the data (solid line) and calculated contributions (dashed line) of the $Ir–O_{support}$ shell; (D) k^1-weighted, phase-corrected, imaginary part and magnitude of the Fourier transform of the data (solid line) and calculated contributions (dashed line) of the Ir–C shell; (E) k^2-weighted, phase-corrected, imaginary part and magnitude of the Fourier transform of the data (solid line) and calculated contributions (dashed line) of the Ir–Al shell; (F) k^2-weighted, phase-corrected, imaginary part and magnitude of the Fourier transform of the data (solid line) and calculated contributions (dashed line) of the $Ir–O_{long}$ shell.

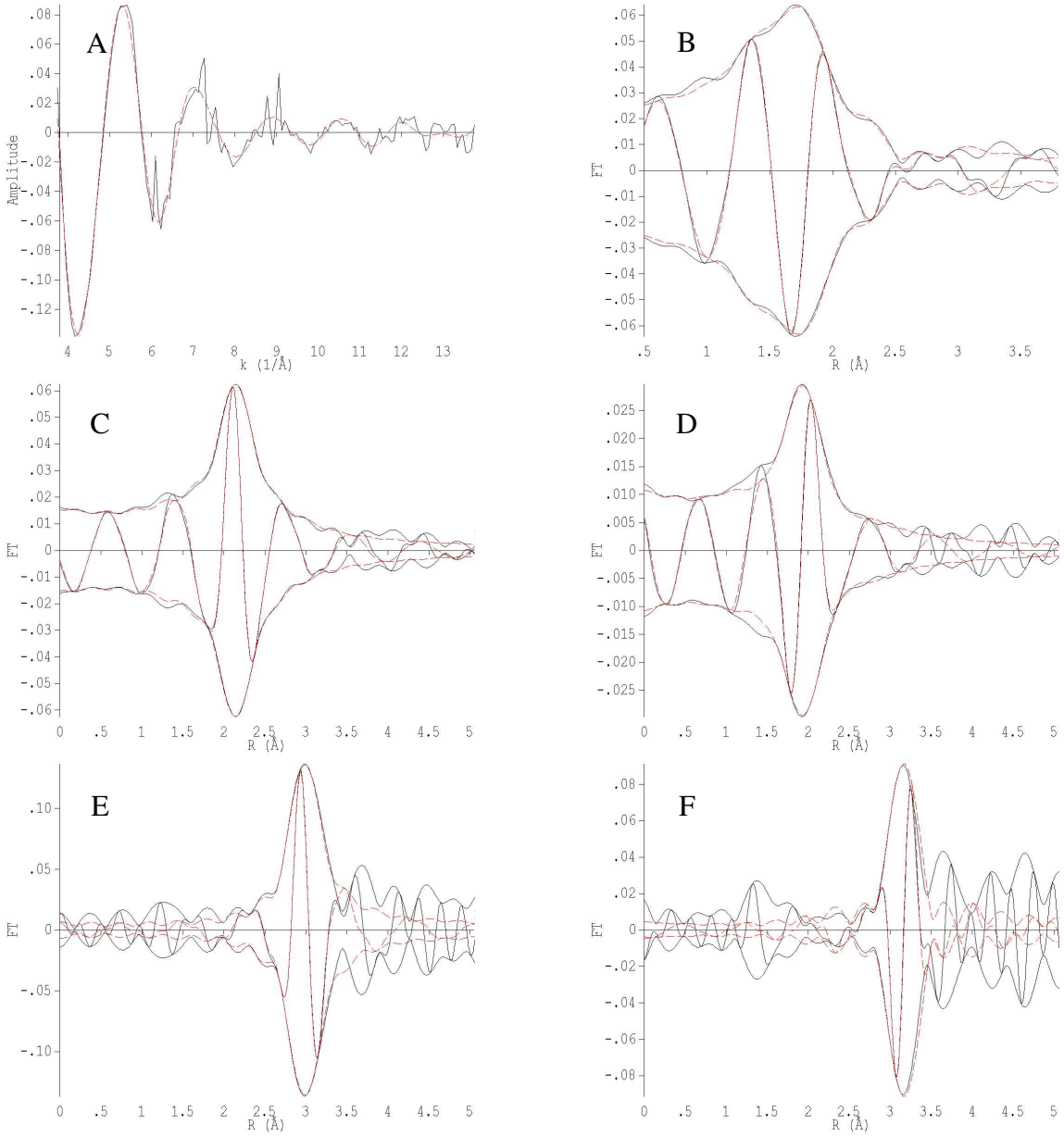

Figure S12. EXAFS data characterizing highly dealuminated zeolite Y-supported iridium complex formed by treatment of the zeolite-supported $Ir(C_2H_4)_2$ sample in flowing C_2H_4 + H_2 at 298 K for 2 h: (A) k^1-weighted EXAFS function, $k^1(\chi)$ (solid line) and sum of the calculated contributions (dashed line); (B) k^1-weighted imaginary part and magnitude of the Fourier transform of the data (solid line) and sum of the calculated contributions (dashed line); (C) k^1-weighted, phase-corrected, imaginary part and magnitude of the Fourier transform of the data (solid line) and calculated contributions (dashed line) of the Ir–$O_{support}$ shell; (D) k^1-weighted, phase-corrected, imaginary part and magnitude of the Fourier transform of the data (solid line) and calculated contributions (dashed line) of the Ir–C shell; (E) k^2-weighted, phase-corrected, imaginary part and magnitude of the Fourier transform of the data (solid line) and calculated contributions (dashed line) of the Ir–Al shell; (F) k^2-weighted, phase-corrected, imaginary part and magnitude of the Fourier transform of the data (solid line) and calculated contributions (dashed line) of the Ir–C_{long} shell.

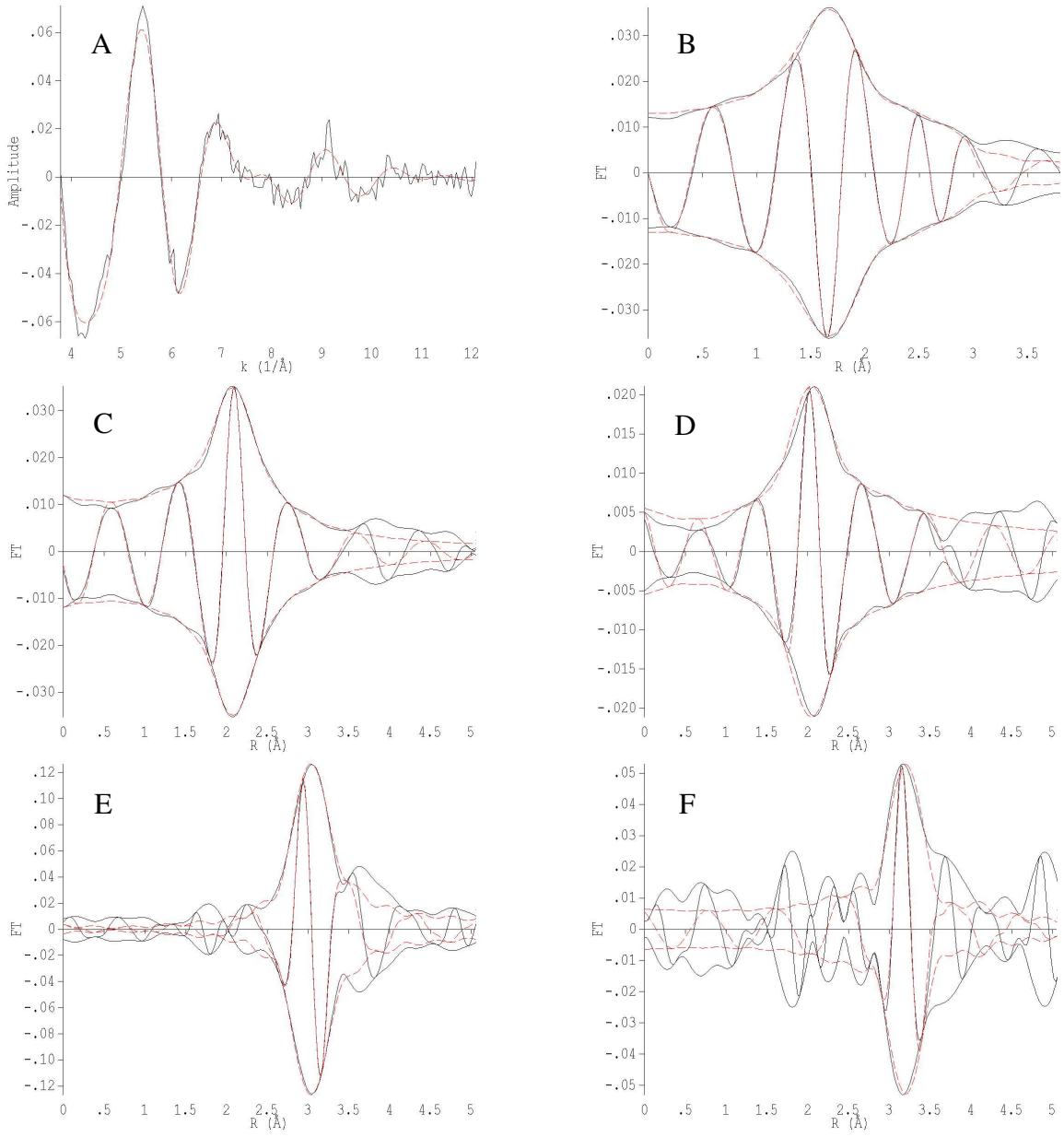

Figure S13. EXAFS data characterizing highly dealuminated zeolite Y-supported iridium complex formed by treatment of the zeolite-supported $Ir(C_2H_4)_2$ sample in flowing H_2 at 298 K for 20 min: (A) k^1-weighted EXAFS function, $k^1(\chi)$ (solid line) and sum of the calculated contributions (dashed line); (B) k^1-weighted imaginary part and magnitude of the Fourier transform of the data (solid line) and sum of the calculated contributions (dashed line); (C) k^1-weighted, phase-corrected, imaginary part and magnitude of the Fourier transform of the data (solid line) and calculated contributions (dashed line) of Ir–$O_{support}$ shell; (D) k^1-weighted, phase-corrected, imaginary part and magnitude of the Fourier transform of the data (solid line) and calculated contributions (dashed line) of the Ir–C shell; (E) k^2-weighted, phase-corrected, imaginary part and magnitude of the Fourier transform of the data (solid line) and calculated contributions (dashed line) of the Ir–Al shell; (F) k^2-weighted, phase-corrected, imaginary part and magnitude of the Fourier transform of the data (solid line) and calculated contributions (dashed line) of the Ir–C_{long} shell.

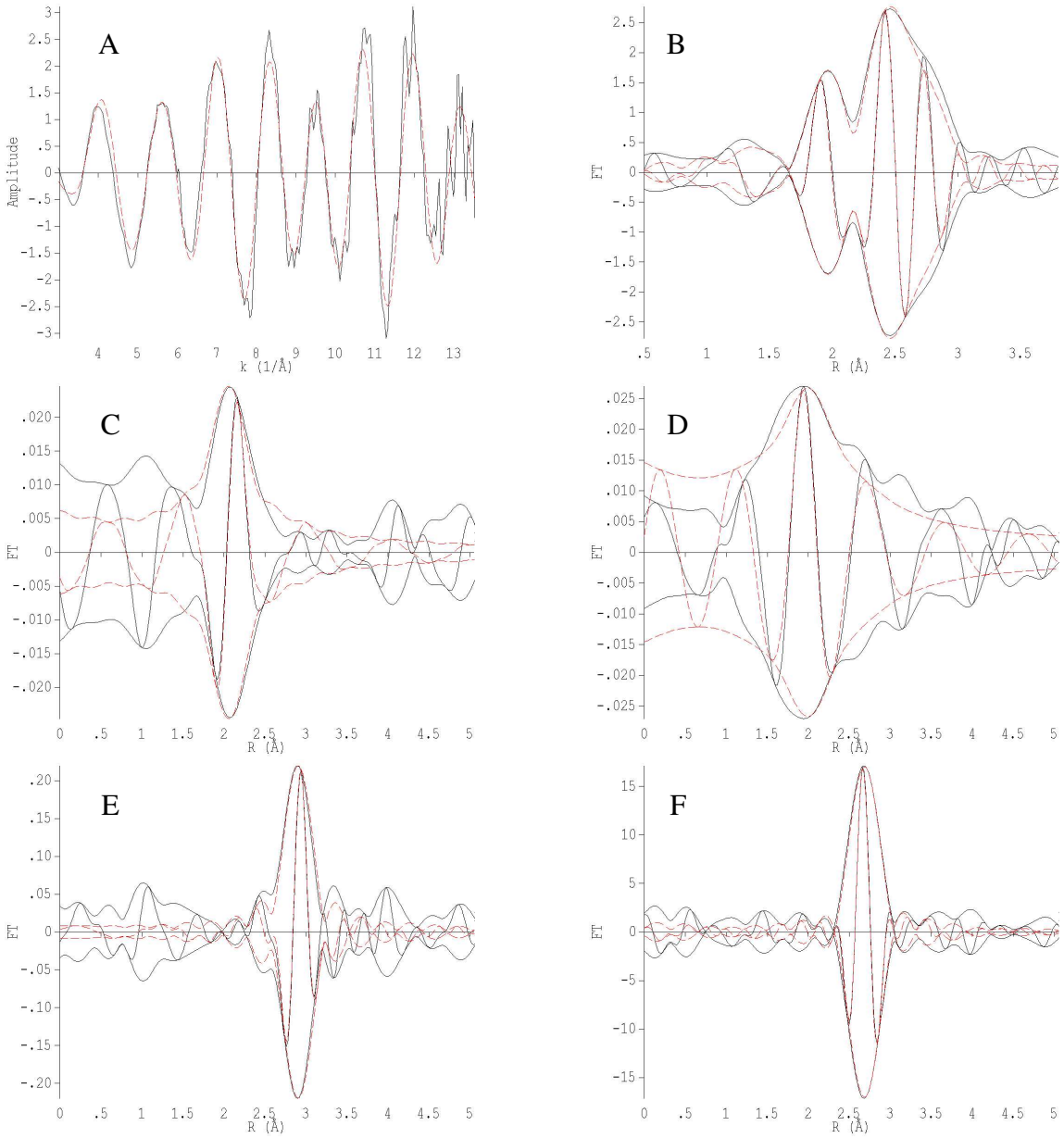

Figure S14. EXAFS data characterizing highly dealuminated zeolite Y-supported Ir_4 clusters prepared from treatment of the zeolite-supported $Ir(C_2H_4)_2$ sample in flowing H_2 at 353 K for 1 h: (A) k^3-weighted EXAFS function, $k^3(\chi)$ (solid line) and sum of the calculated contributions (dashed line); (B) k^3-weighted imaginary part and magnitude of the Fourier transform of the data (solid line) and sum of the calculated contributions (dashed line); (C) k^1-weighted, phase-corrected, imaginary part and magnitude of the Fourier transform of the data (solid line) and calculated contributions (dashed line) of Ir-$O_{support}$ shell; (D) k^1-weighted, phase-corrected, imaginary part and magnitude of the Fourier transform of the data (solid line) and calculated contributions (dashed line) of Ir-C shell; (E) k^2-weighted, phase-corrected, imaginary part and magnitude of the Fourier transform of the data (solid line) and calculated contributions (dashed line) of Ir-Al shell; (F) k^3-weighted, phase-corrected, imaginary part and magnitude of the Fourier transform of the data (solid line) and calculated contributions (dashed line) of Ir-Ir shell.

Table S2: Summary of EXAFS fit parameters characterizing the highly dehydroxylated MgO-supported iridium Complex after different treatments.

		N	*R*(Å)	$10^3 \times \Delta\sigma^2$ (Å^2)	ΔE_0(eV)	*k*-range		*R*-range		Error in EXAFS function[b]	Goodness of fit[c]
As prepared sample	Ir-$O_{support}$	2.0	2.00	8.1	-8.0	3.86	13.09	0.5	3.8	0.001	1.3
	Ir-C	4.0	2.12	6.3	-3.1						
	Ir-Mg	1.9	3.06	9.5	-5.8						
	Ir-O_{long}	3.2	3.70	9.2	-8.0						
After 2 h of ethene hydrogenation reaction at 298 K	Ir-$O_{support}$	2.2	2.03	12	-7.9	3.86	13.61	0.5	3.8	0.001	4.1
	Ir-C	3.8	2.10	5.2	-3.5						
	Ir-Mg	2.0	2.99	12	-1.0						
	Ir-O_{long}	3.5	3.63	9.9	-2.8						
After 2 h in H_2 flow at 298 K	Ir-$O_{support}$	1.9	2.12	3.9	-3.4	3.81	13.15	0.5	4.0	0.0005	9.4
	Ir-C	3.6	2.06	6.1	-8.0						
	Ir-Mg	2.5	2.98	11	0.35						
	Ir-O_{long}	4.1	3.66	11	-4.74						
After 1 h in H_2 flow at 353 K (Model I in Table S3)	Ir-$O_{support}$	1.2	2.33	1.4	8.0	3.22	12.59	0.5	3.8	0.0007	2.9
	Ir-C	0.78	2.14	1.5	3.9						
	Ir-Mg	2.1	3.17	2.1	-5.5						
	Ir-O_{long}	2.8	3.39	1.4	-4.4						
	Ir-Ir	2.9	2.73	4.4	4.2						

[a] Notation: $O_{support}$, oxygen from support; O_{long}, oxygen from support in a distance longer than bonding distance; *N*, coordination number; *R*, distance between absorber and backscatterer atoms; $\Delta\sigma^2$, Debye-Waller factor; ΔE_0, Inner potential correction. Error bounds (accuracies) characterizing the structural parameters, obtained by EXAFS spectroscopy are estimated to be as follows: *N*, ± 20%; *R*, ± 0.02Å; $\Delta\sigma^2$, ± 20%; and ΔE_0, ± 20%. [b] The error in the data was calculated as the root mean square of the value obtained from the subtraction of smoothed χ data from the background-subtracted experimental χ values. [c] Goodness of fit values were calculated with the software XDAP, as follows: $goodness\ of\ fit = \frac{\nu}{NPTS(\nu - N_{free})} \sum_{i=1}^{NPTS} \left(\frac{\chi_{exp,i} - \chi_{model,i}}{\sigma_{exp,i}} \right)^2$ The terms χ_{model} and χ_{exp} are the model and experimental EXAFS values, respectively; σ_{exp} is the error in the experimental results; ν is the number of independent data points in the fit range; and NPTS is the actual number of data points in the fit range; N_{free} is the number of free parameters. [d] The number of statistically justified parameters was calculated by using the Nyquist theorem, as follows: number of justified parameters = $n = (2\Delta k \Delta R/\pi) + 2$, where Δk and ΔR are the *k*- and *R*- ranges used the fitting.

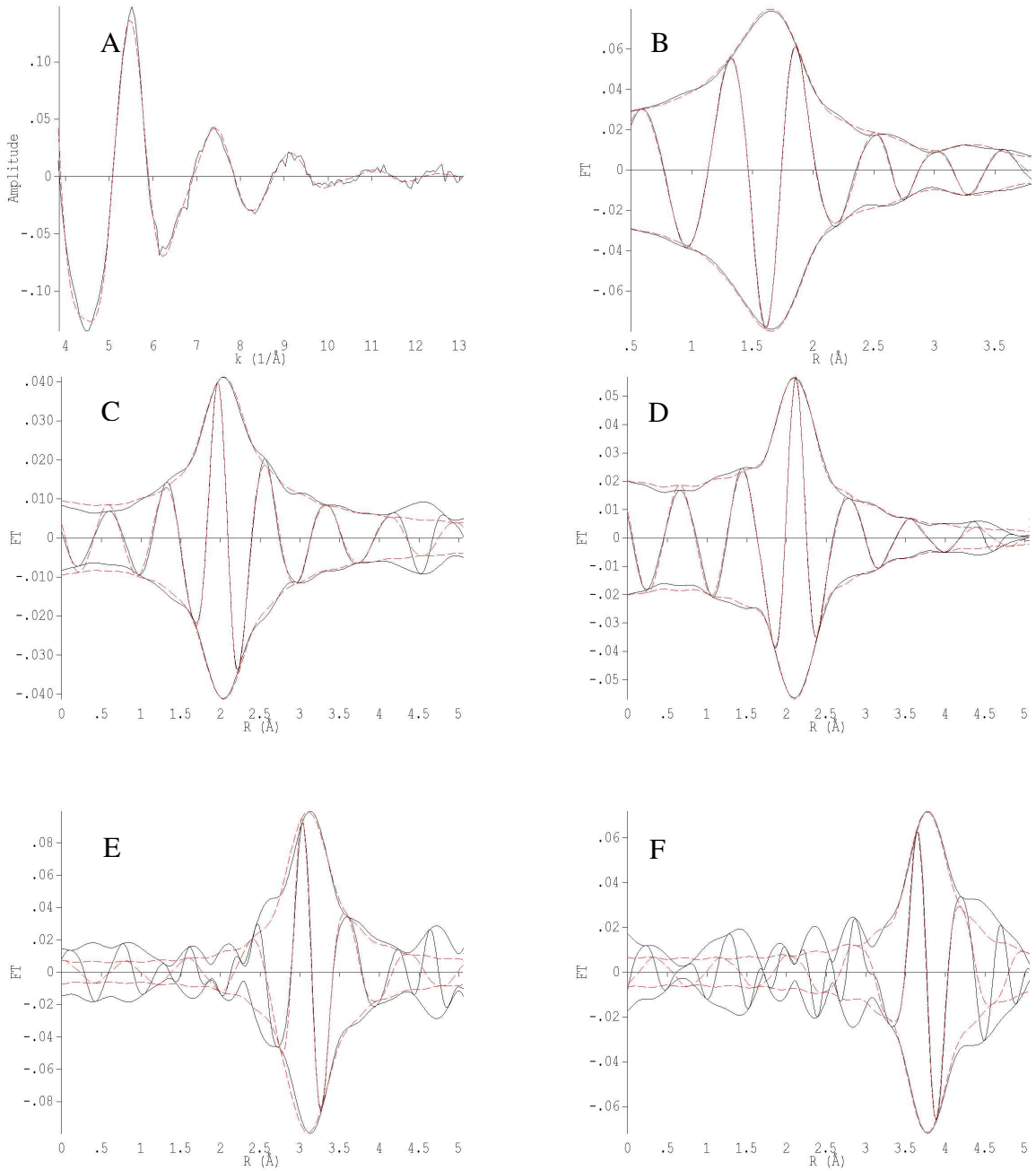

Figure S15. EXAFS data characterizing initially prepared highly dehydroxylated MgO-supported iridium complex formed by adsorption of $Ir(C_2H_4)_2(acac)$ on MgO: (A) k^1-weighted EXAFS function, $k^1(\chi)$ (solid line) and sum of the calculated contributions (dashed line); (B) k^1-weighted imaginary part and magnitude of the Fourier transform of the data (solid line) and sum of the calculated contributions (dashed line); (C) k^1-weighted, phase-corrected, imaginary part and magnitude of the Fourier transform of the data (solid line) and calculated contributions (dashed line) of Ir-$O_{support}$ shell; (D) k^1-weighted, phase-corrected, imaginary part and magnitude of the Fourier transform of the data (solid line) and calculated contributions (dashed line) of Ir-C shell; (E) k^2-weighted, phase-corrected, imaginary part and magnitude of the Fourier transform of the data (solid line) and calculated contributions (dashed line) of Ir-Mg shell; (F) k^2-weighted, phase-corrected, imaginary part and magnitude of the Fourier transform of the data (solid line) and calculated contributions (dashed line) of Ir-O_{long} shell.

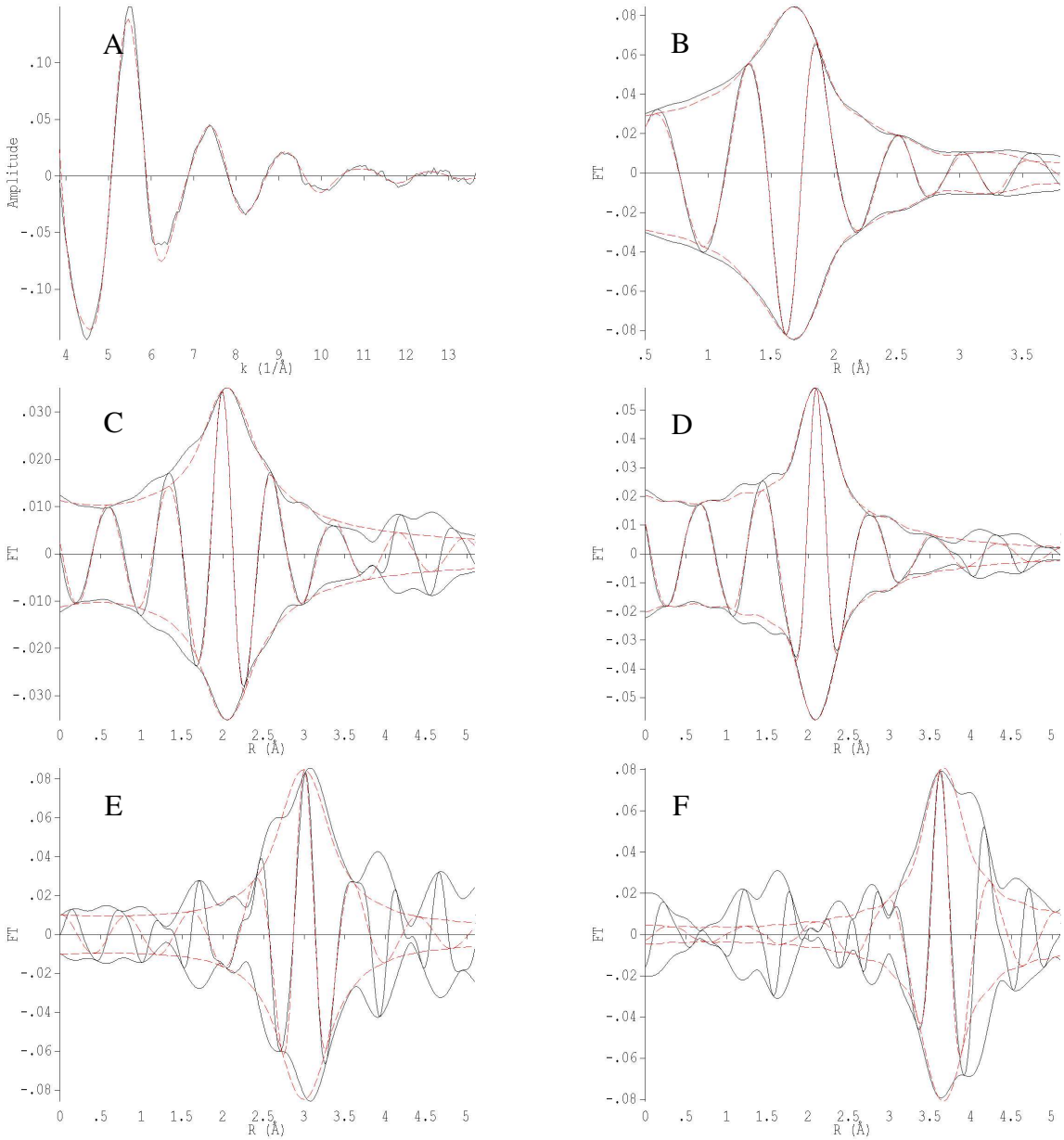

Figure S16. EXAFS data characterizing highly dehydroxylated MgO-supported iridium complex prepared by treatment of the MgO-supported $Ir(C_2H_4)_2$ sample in flowing $C_2H_4 + H_2$ (during ethene hydrogenation catalysis) at 298 K for 2 h: (A) k^1-weighted EXAFS function, $k^1(\chi)$ (solid line) and sum of the calculated contributions (dashed line); (B) k^1-weighted imaginary part and magnitude of the Fourier transform of the data (solid line) and sum of the calculated contributions (dashed line); (C) k^1-weighted, phase-corrected, imaginary part and magnitude of the Fourier transform of the data (solid line) and calculated contributions (dashed line) of Ir-$O_{support}$ shell; (D) k^1-weighted, phase-corrected, imaginary part and magnitude of the Fourier transform of the data (solid line) and calculated contributions (dashed line) of Ir-C shell; (E) k^2-weighted, phase-corrected, imaginary part and magnitude of the Fourier transform of the data (solid line) and calculated contributions (dashed line) of Ir-Mg shell; (F) k^2-weighted, phase-corrected, imaginary part and magnitude of the Fourier transform of the data (solid line) and calculated contributions (dashed line) of Ir-O_{long} shell.

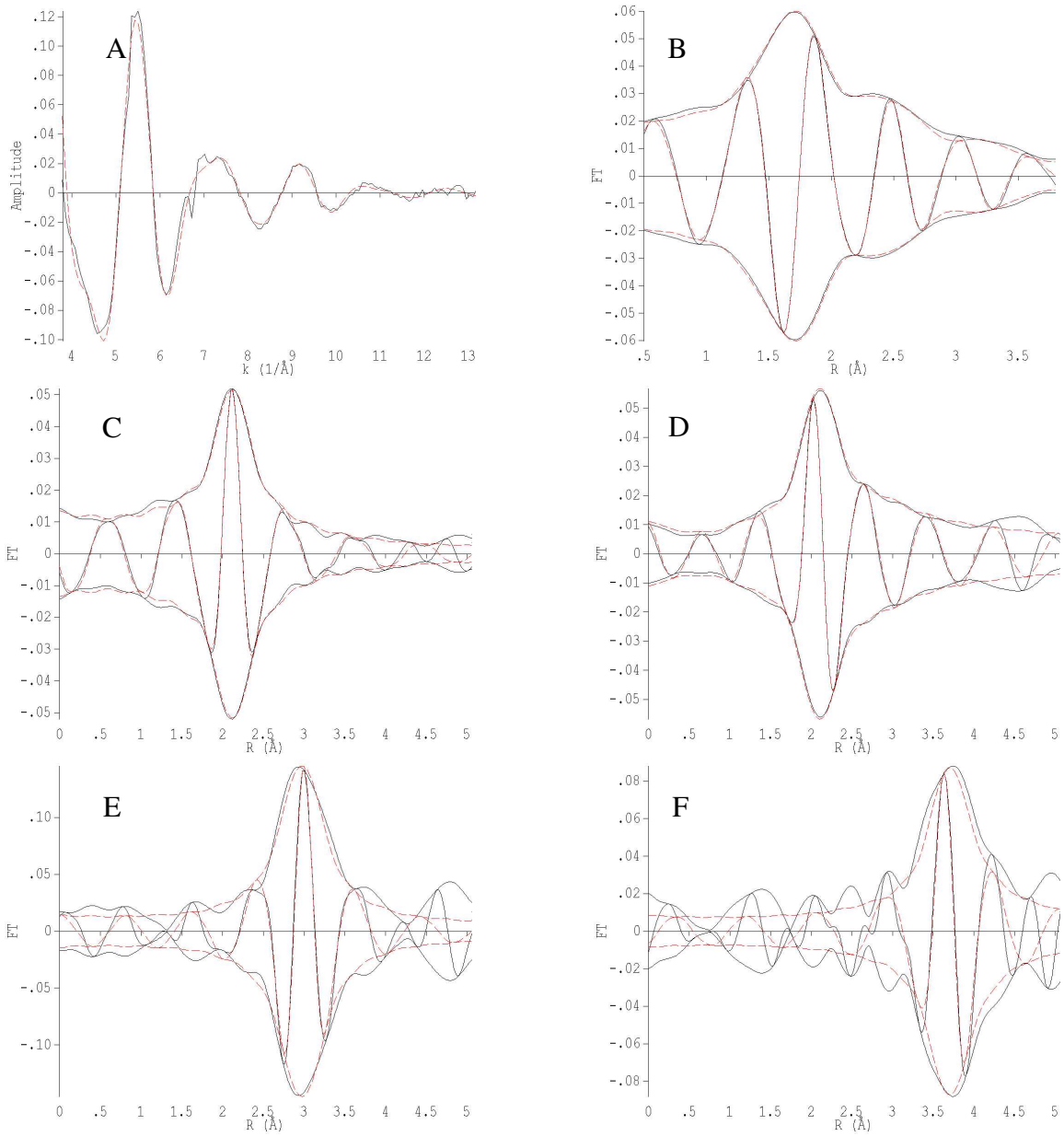

Figure S17. EXAFS data characterizing highly dehydroxylated MgO-supported iridium complex prepared by treatment of the MgO-supported $Ir(C_2H_4)_2$ sample in flowing H_2 at 298 K for 2 h: (A) k^1-weighted EXAFS function, $k^1(\chi)$ (solid line) and sum of the calculated contributions (dashed line); (B) k^1-weighted imaginary part and magnitude of the Fourier transform of the data (solid line) and sum of the calculated contributions (dashed line); (C) k^1-weighted, phase-corrected, imaginary part and magnitude of the Fourier transform of the data (solid line) and calculated contributions (dashed line) of Ir-$O_{support}$ shell; (D) k^1-weighted, phase-corrected, imaginary part and magnitude of the Fourier transform of the data (solid line) and calculated contributions (dashed line) of Ir-C shell; (E) k^2-weighted, phase-corrected, imaginary part and magnitude of the Fourier transform of the data (solid line) and calculated contributions (dashed line) of Ir-Mg shell; (F) k^2-weighted, phase-corrected, imaginary part and magnitude of the Fourier transform of the data (solid line) and calculated contributions (dashed line) of Ir-O_{long} shell.

Materials and Sample Preparation. Sample synthesis and handling were performed with the exclusion of moisture and air. H_2 was supplied by Airgas (99.999%) and was purified by passage through traps containing reduced Cu/Al_2O_3 and activated zeolite 4A to remove traces of O_2 and moisture, respectively. Helium (Airgas, 99.999%) and C_2H_4 (Airgas, 99.99%) were purified by passage through similar traps. CO (Matheson, 99.999%), in a 10% mixture in helium, was purified by passage through a trap containing activated α-Al_2O_3 particles and zeolite 4A to remove any traces of metal carbonyls from high-pressure gas cylinders and moisture, respectively. Deuterium (99.8% D_2) was purchased from Cambridge Isotope Laboratories. The highly dealuminated HY zeolite (DAY zeolite) (Zeolyst International, CBV760), with a Si/Al atomic ratio of approximately 30, was calcined in O_2 at 773 K for 4 h and was evacuated for 16 h at 773 K. MgO (EM Science) was mixed with deionized water to form a paste, which was dried overnight in air at 393 K. The resultant solid was ground and treated in O_2 as the temperature was ramped linearly from room temperature to 973 K and then held for 2 h, resulting in a high degree of dehydroxylation.[4] After calcination, the samples of DAY zeolite and MgO were isolated, and each was stored in an argon-filled glove box (MBraun, with H_2O level less than 0.5 ppm and O_2 level less than 5 ppm) until it was used. *n*-Pentane solvent (Fisher, 99%) was dried and purified by column chromatography (Grubbs apparatus, MBraun SPS) in the presence of argon.

The precursor $Ir(C_2H_4)_2(acac)$ [acetylacetonatobis(ethene)-iridium(I)] was synthesized as described elsewhere,[5] with a detailed characterization by X-ray diffraction crystallography, ^1H and ^{13}C NMR, Raman, and IR spectroscopies. To prepare the supported iridium complex, $Ir(C_2H_4)_2(acac)$ and the calcined zeolite DAY or MgO powder in a Schlenk flask were slurried in a dried *n*-pentane that was initially at ice temperature. The stirred slurry was warmed to room temperature, and, after 1 day, the solvent was removed by evacuation for 1 day, so that all the iridium remained in the zeolite. The resultant solids, containing 1 wt% Ir, were stored in the argon-filled glove box.

IR Spectroscopy. A Bruker IFS 66v/S spectrometer with a spectral resolution of 2 cm^{-1} was used to collect transmission IR spectra of power samples. Approximately 30 mg of solid sample inside glove box was pressed into a thin wafer and loaded into a cell that serves a flow reactor (In-situ Research Institute, Inc., South Bend, IN). The cell was sealed and connected to a flow system that allowed recording of spectra while the reactant gases flowed through the cell at reaction temperature. Each spectrum is the average of 64 scans.

Electron Microscopy Sample Handling. To protect the air-sensitive catalysts from exposure to the atmosphere, the microscopy samples were prepared by using a lacey carbon, 300 mesh, copper grid (Ted-Pella) that was dipped into the powder sample in an argon-filled glovebox (MBraun) with a moisture level less than 0.5 ppm and an oxygen level less than 5 ppm. After shaking off of the excess powder on the grid, the grid was transferred to an Eppendorf tube and sealed with Parafilm. The tubes were then placed into stainless-steel Swagelok tubes and the ends were clamped together and sealed with O-rings for air exclusion in preparation for transfer to the microscope facility. In the microscope facility, at the closest possible distance to the

equipment, an argon-filled glovebag (Glas-Col) was set up and purged 5 times with ultra-high-purity argon (Praxair, Grade 5.0) prior to the opening of the sample tubes and loading the TEM grid on the microscope holder, which were carried out under the blanket of flowing argon. After briefly opening the glovebag, the holder was inserted to the microscope and the pumping used to evacuate the microscope chamber was initiated within 5 s.

HAADF-STEM Imaging. Images of the sample were obtained with a JEOL JEM-2100F electron microscope at University of California, Davis. The microscope is equipped with a FEG, operating at 200 kV, with a CEOS hexapole probe (STEM) aberration corrector, having a probe size of 0.27 nm at full-width-half-maximum (FWHM). The images were captured by a HAADF detector with a collection semi-angle of 75–200 mrad and a probe convergence semi-angle of 17.1 mrad.

Prior to imaging the sample, the aberration corrector was aligned with Pt/Ir on holey carbon standard sample (SPI supplies) until atomic resolution on the metal particles was achieved and lattice spacing of the metals in the standard sample was confirmed.

Cluster Size Measurement on HAADF-STEM Images. A total of 226 and 288 clusters were analyzed for size measurement of iridium species on MgO and DAY zeolite, respectively. For each cluster, an intensity profile was obtained by using the Digital Micrograph software (Gatan), as depicted in Figure S21. Line profiles were then transferred to OriginPro for baseline correction. Background subtracted profiles of the clusters were fitted to a Gaussian distribution function in OriginPro, and full-width-half-maximum (FWHM) values of the fitted peak were reported as the diameter of each iridium cluster metal framework.

Average cluster diameters are reported in the main text with a standard deviation for each sample. Standard blurring effects in STEM images—associated with electron beam probe size, vibration (instabilities), movement of atoms under the influence of the beam, irradiation effects, off-focus, beam broadening, and so forth[6]—are expected to cause a slight overestimation of the size of the extremely small clusters, as well as some broadening of the overall size distribution.

Examples of the steps in cluster size measurement are given in Figure S21 for the HAADF-STEM image of the catalyst formed by treatment of $Ir(C_2H_4)_2$ species supported on DAY zeolite with flowing H_2 at 353 K for 1 h.

Ethylene Hydrogenation Catalysis. Ethylene hydrogenation catalysis was carried out in a conventional laboratory once-through tubular plug-flow reactor. The catalyst (typically, 30 mg for the DAY zeolite-supported catalysts and 150 mg for the MgO-supported catalyst) was diluted with 10 g of inert, nonporous α-Al_2O_3 loaded into the reactor in a glove box. The feed partial pressure was 333 mbar for C_2H_4 and 666 mbar for H_2 with a total flow rate of 60 mL/min and total pressure being atmospheric. The temperature was 298 ± 1 K.

Products were analyzed by gas chromatography by use of an HP-6890 gas chromatograph equipped with a 50 m × 0.53 mm DB-624 capillary column (J & W Scientific) and a flame-ionization detector. The effluent gas from the reactor was sampled every 12 min and analyzed. Intrinsic catalytic activities (expressed as moles of ethene converted (moles of iridium × s), the turnover frequency, TOF) were determined by operation of the reactor in the differential conversion range (conversion <5%). TOF values were calculated by assuming that all the Ir atoms in both mononuclear complexes and Ir_4 clusters are accessible to the reactants. As shown

in Figure S8, the activity of each of the catalysts decreased with time on stream as a consequence of modification of the active sites. In general, the rate of deactivation was higher for the zeolite-supported samples, probably because of the formation of small amounts of heavier hydrocarbons, as evidenced by mass spectra of the products; these heavier hydrocarbons could poison the metal species by irreversible adsorption. To eliminate the effect of the deactivation, the activity of each catalyst was extrapolated to time on stream = 0 from the corresponding TOF *vs.* time on stream plots. At these low times on stream, the only observed reaction product was ethane.

Isotopic H_2/D_2 Exchange Experiments. Meaurements of mass spectra were carried out to determine the products of the reaction in tubular plug-flow reactors identical to those used for the ethene hydrogenation measurements. The catalyst (20 mg for measurements without C_2H_4 in the feed or 30 mg for measurements with C_2H_4) was diluted with 5 g of inert, nonporous α-Al_2O_3 and was loaded into the reactor in an inert-atmosphere glove box. The feed consisting of C_2H_4, H_2, and D_2 (the partial pressure of each was 200 mbar balanced in helium) with the total flow rate being 100 mL(NTP)/min and the total pressure being atmospheric. The temperature was 298 ± 1 K, controlled with a cooling jacket filled with water. Mass spectra of the gases introduced into the flow system and the effluents produced by reaction were measured with an online Balzers OmniStar mass spectrometer running in multi-ion monitoring mode. Specifically, changes in the signal intensities of H_2 (*m/e* = 2), D_2 (*m/e* = 4), HD (*m/e* = 3), CO (*m/e* =28), C_2H_4 (*m/e* = 26, 27, and 28), C_2H_6 (*m/e* = 26, 27, 28, and 30), C_4H_8 (*m/e* = 41 and 43), and C_4H_{10} (*m/e* =55 and 56) were recorded. The reported intensity values were corrected by subtracting background intensities recorded while the reaction gas mixture was bypassing the flow reactor containing the catalyst. The HD exchange was measured at room temperature for times on stream <10 min, for which the nuclearity of the iridium complexes initially present as single-atom complexes was maintained, as demonstrated by EXAFS spectroscopy. We emphasize that the amount of H_2 and D_2 consumed in the formation of ethane was, under the selected conditions, negligible with respect to the HD exchange.

X-ray Absorption Spectroscopy. Most of the X-ray absorption spectra were recorded at X-ray beam line MR-CAT at the Advanced Photon Source (APS) at the Argonne National Laboratory. The storage ring electron energy and ring currents were 7.0 GeV and 105 mA, respectively. The cryogenic double crystal Si(111) monochromator was detuned by 20–25% at the Ir L_{III} edge to minimize the effects of higher harmonics in the X-ray beam.

In an N_2 filled glovebox at the APS, powder samples were loaded into a flow through cell,[7] which was sealed in the inert atmosphere. The mass of each sample (approximately 0.3 g) was chosen for optimal absorption measurements at the Ir L_{III} edge (11 215 eV) (giving an X-ray absorbance of approximately 2.0 calculated at an energy 50 eV greater than the absorption edge). Spectra were collected in transmission mode with the presence of flowing gases at 1 bar and temperature between 298 K and 353 K.

Table S3: Summary of EXAFS fit parameters characterizing highly dehydroxylated MgO-supported Ir_4 clusters prepared from treatment of the MgO-supported $Ir(C_2H_4)_2$ sample after treatment in flowing H_2 at 353 K for 1 h. Comparison of candidate models.

		N	*R(Å)*	$10^3 \times \Delta\sigma^2$ *(Å²)*	ΔE_0*(eV)*	*k-range (Å⁻¹)*		*R-range (Å²)*		*Error in EXAFS function*[b]	*Goodness of fit*[c]
Model I	Ir-$O_{support}$	1.2	2.33	1.4	8.0	3.22	12.59	0.5	3.8	0.0007	2.9
	Ir-C	0.78	2.14	1.5	3.9						
	Ir-Mg	2.1	3.16	2.1	-5.5						
	Ir-O_{long}	2.8	3.39	1.4	-4.4						
	Ir-Ir	2.9	2.73	4.4	4.2						
Model II	Ir-$O_{support}$	1.6	2.31	4.5	8.0	3.22	12.59	0.5	3.8	0.0007	2.7
	Ir-C	1.0	2.13	0.8	0.2						
	Ir-Mg	1.3	3.14	1.2	-4.5						
	Ir-Ir	3.0	2.73	4.3	4.9						
Model III	Ir-$O_{support}$	1.5	2.31	4.4	4.1	3.22	12.59	0.5	3.8	0.0007	3.4
	Ir-C	1.0	2.14	0.7	-7.6						
	Ir-Mg	1.6	3.11	4.5	-2.0						
	Ir-Ir	2.9	2.73	4.6	4.5						
	Ir-Ir_{2nd}	0.8	3.72	2.5	8.0						

[a] Notation: $O_{support}$, oxygen from support; O_{long}, oxygen from support in a distance longer than bonding distance; Ir-Ir_{2nd}, second shell Ir; *N*, coordination number; *R*, distance between absorber and backscatterer atoms; $\Delta\sigma^2$, Debye-Waller factor; ΔE_0, Inner potential correction. Error bounds (accuracies) characterizing the structural parameters, obtained by EXAFS spectroscopy are estimated to be as follows: *N*, ± 20%; *R*, ± 0.02Å; $\Delta\sigma^2$, ± 20%; and ΔE_0, ± 20%. [b] The error in the data was calculated as the root mean square of the value obtained from the subtraction of smoothed χ data from the background-subtracted experimental χ values. [c] Goodness of fit values were calculated with the software XDAP, as follows:

$$goodness\ of\ fit = \frac{\nu}{NPTS\left(\nu - N_{free}\right)} \sum_{i=1}^{NPTS} \left(\frac{\chi_{\exp,i} - \chi_{\mathrm{model},i}}{\sigma_{\exp,i}} \right)^2$$

The terms χ_{model} and χ_{exp} are the model and experimental EXAFS values, respectively; σ_{exp} is the error in the experimental results; ν is the number of independent data points in the fit range; and NPTS is the actual number of data points in the fit range; N_{free} is the number of free parameters. [d] The number of statistically justified parameters was calculated by using the Nyquist theorem, as follows: number of justified parameters = $n = (2\Delta k \Delta R/\pi) + 2$, where Δk and ΔR are the *k*- and *R*- ranges used the fitting.

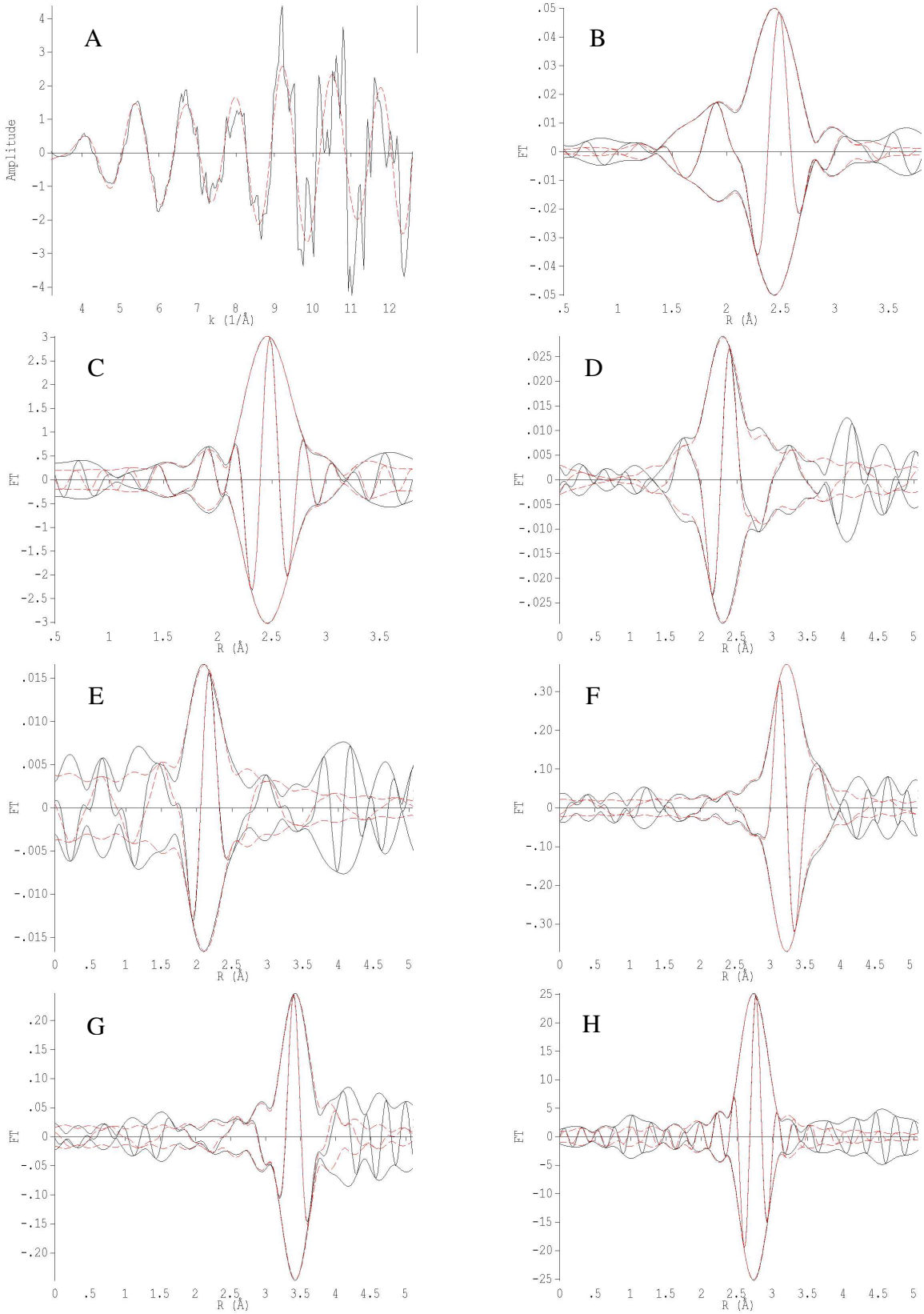

Figure S18. EXAFS data characterizing highly dehydroxylated MgO-supported Ir_4 clusters prepared from treatment of the $Ir(C_2H_4)_2$_MgO catalyst in flowing H_2 at 353 K for 1 h, fitting for model I: (A) k^3-

weighted EXAFS function, $k^3(\chi)$ (solid line) and sum of the calculated contributions (dashed line); (B) k^1-weighted imaginary part and magnitude of the Fourier transform of the data (solid line) and sum of the calculated contributions (dashed line); (C) k^3-weighted imaginary part and magnitude of the Fourier transform of the data (solid line) and sum of the calculated contributions (dashed line); (D) k^1-weighted, phase-corrected, imaginary part and magnitude of the Fourier transform of the data (solid line) and calculated contributions (dashed line) of Ir-$O_{support}$ shell; (E) k^1-weighted, phase-corrected, imaginary part and magnitude of the Fourier transform of the data (solid line) and calculated contributions (dashed line) of Ir-C shell; (F) k^2-weighted, phase-corrected, imaginary part and magnitude of the Fourier transform of the data (solid line) and calculated contributions (dashed line) of Ir-Mg shell; (G) k^2-weighted, phase-corrected, imaginary part and magnitude of the Fourier transform of the data (solid line) and calculated contributions (dashed line) of Ir-O_{long} shell; (H) k^3-weighted, phase-corrected, imaginary part and magnitude of the Fourier transform of the data (solid line) and calculated contributions (dashed line) of Ir-Ir shell.

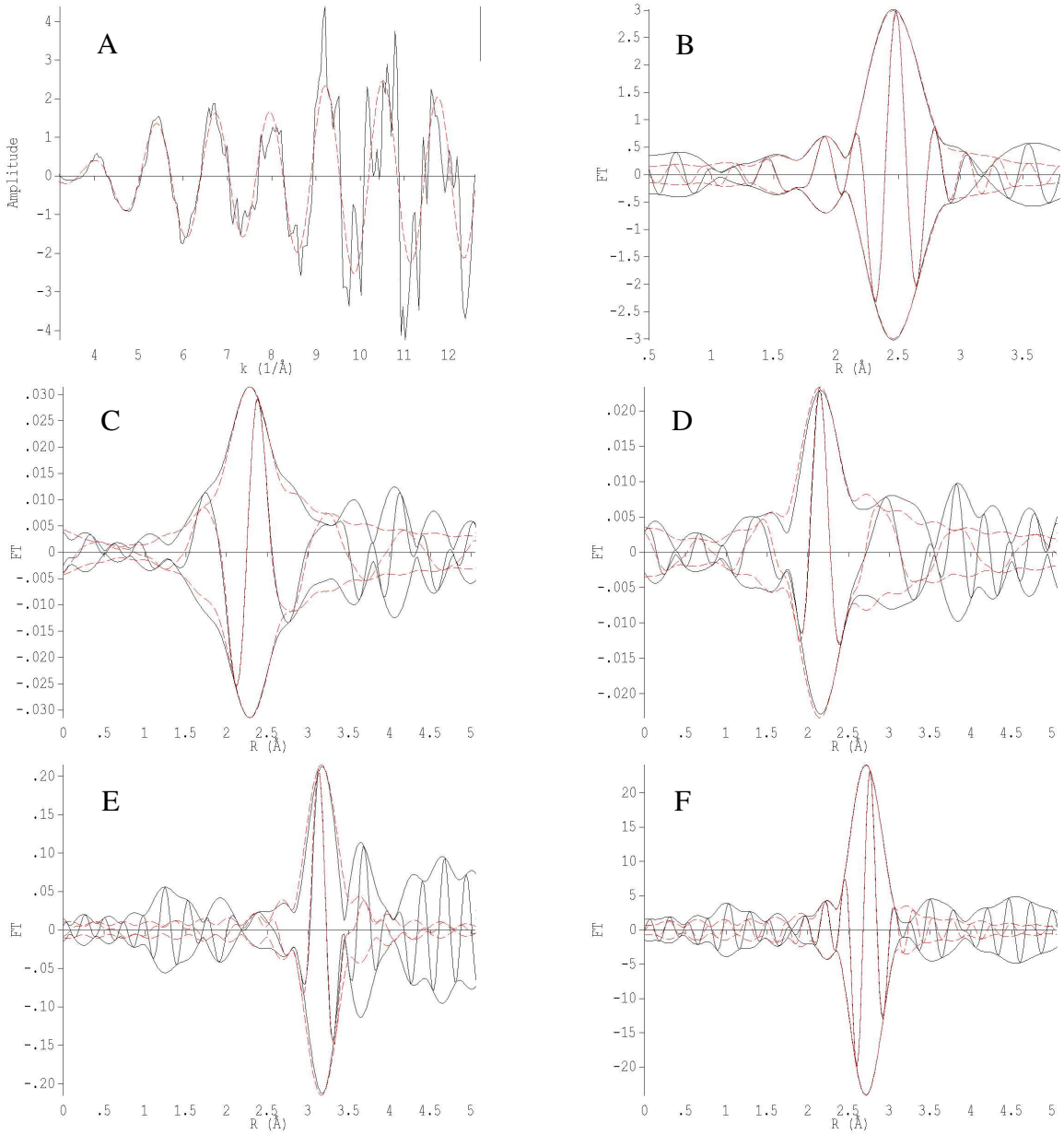

Figure S19. EXAFS data characterizing highly dehydroxylated MgO-supported Ir_4 clusters prepared from treatment of the $Ir(C_2H_4)_2$_MgO catalyst in flowing H_2 at 353 K for 1 h, fitting for model II: (A) k^3-weighted EXAFS function, $k^3(\chi)$ (solid line) and sum of the calculated contributions (dashed line); (B) k^3-weighted imaginary part and magnitude of the Fourier transform of the data (solid line) and sum of the calculated contributions (dashed line); (C) k^1-weighted, phase-corrected, imaginary part and magnitude of the Fourier transform of the data (solid line) and calculated contributions (dashed line) of Ir-$O_{support}$ shell; (D) k^1-weighted, phase-corrected, imaginary part and magnitude of the Fourier transform of the data (solid line) and calculated contributions (dashed line) of Ir-C shell; (E) k^2-weighted, phase-corrected, imaginary part and magnitude of the Fourier transform of the data (solid line) and calculated contributions (dashed line) of Ir-Mg shell; (F) k^3-weighted, phase-corrected, imaginary part and magnitude of the Fourier transform of the data (solid line) and calculated contributions (dashed line) of Ir-Ir shell.

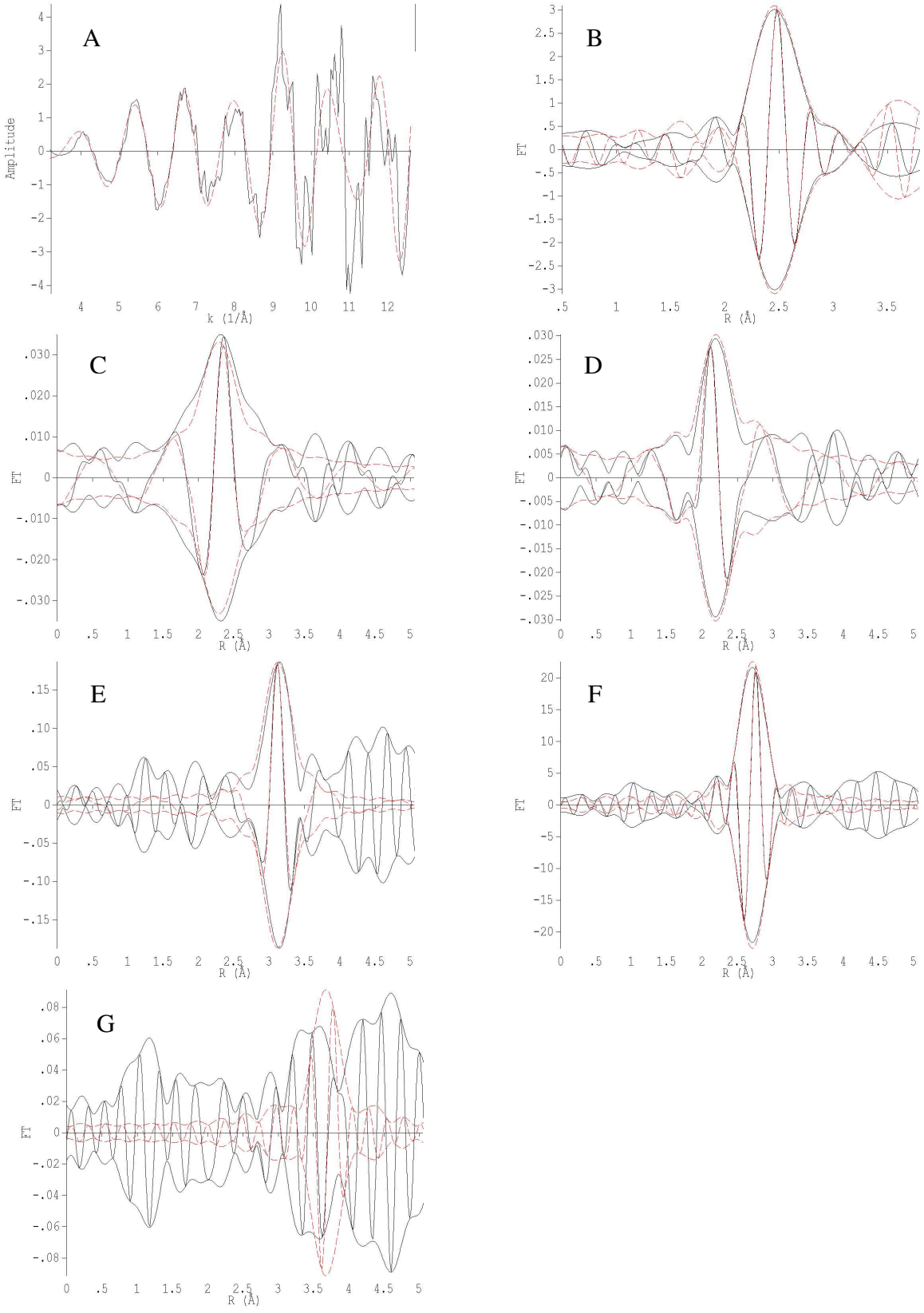
A
Amplitude
k (1/Å)
B
FT
R (Å)
C
FT
R (Å)
D
FT
R (Å)
E
FT
R (Å)
F
FT
R (Å)
G
FT
R (Å)

Figure S20. EXAFS data characterizing highly dehydroxylated MgO-supported Ir_4 clusters prepared from treatment of the $Ir(C_2H_4)_2$_MgO catalyst in flowing H_2 at 353 K for 1 h, fitting for model III: (A) k^3-weighted EXAFS function, $k^3(\chi)$ (solid line) and sum of the calculated contributions (dashed line); (B) k^3-weighted imaginary part and magnitude of the Fourier transform of the data (solid line) and sum of the calculated contributions (dashed line); (C) k^1-weighted, phase-corrected, imaginary part and magnitude of the Fourier transform of the data (solid line) and calculated contributions (dashed line) of Ir-$O_{support}$ shell; (D) k^1-weighted, phase-corrected, imaginary part and magnitude of the Fourier transform of the data (solid line) and calculated contributions (dashed line) of Ir-C shell; (E) k^2-weighted, phase-corrected, imaginary part and magnitude of the Fourier transform of the data (solid line) and calculated contributions (dashed line) of Ir-Mg shell; (F) k^2-weighted, phase-corrected, imaginary part and magnitude of the Fourier transform of the data (solid line) and calculated contributions (dashed line) of Ir-Ir shell; (G) k^3-weighted, phase-corrected, imaginary part and magnitude of the Fourier transform of the data (solid line) and calculated contributions (dashed line) of Ir-Ir_{2nd} shell.

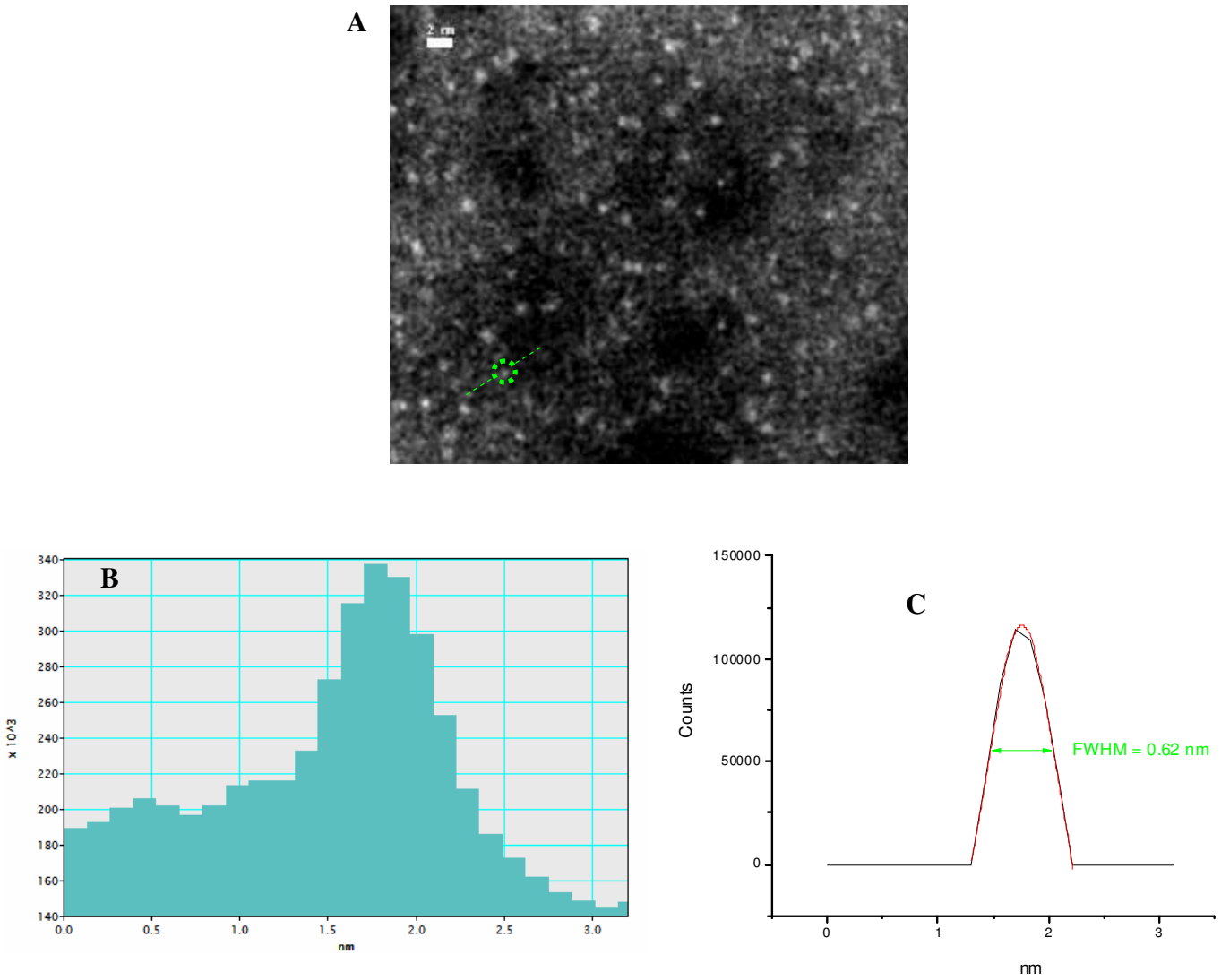

Figure S21: (A) An example cluster circled in green and line drawn across the cluster for generation of intensity profile on HAADF-STEM image of the catalyst formed by treatment of $Ir(C_2H_4)_2$ species supported on DAY zeolite with flow of H_2 at 353 K for 1 h. (B) Intensity line profile created by Digital Micrograph (Gatan) on the example cluster. (C) Background subtracted line profile (black), Gaussian fit (red) for the example cluster (OriginPro). Full-width-half-maximum reported as diameter of cluster metal framework.

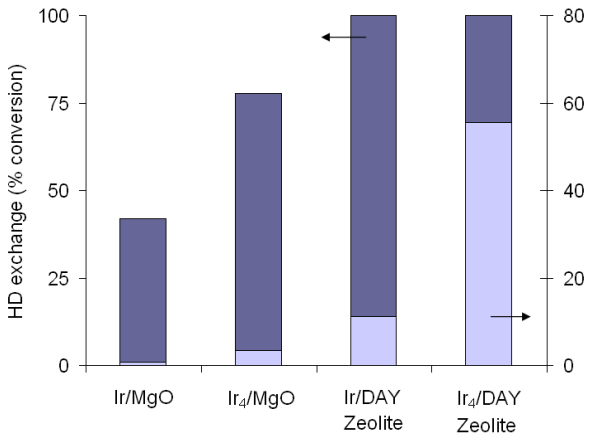

Figure S22. Fractional conversion relative to equilibrium for the isotopic exchange of H_2 and D_2 on various supported iridium catalysts: mononuclear iridium species on MgO, Ir/MgO; iridium clusters well approximated as Ir_4 on MgO (Ir_4/MgO); mononuclear iridium species on DAY zeolite, Ir/DAY zeolite; and approximately tetranuclear iridium species on DAY zeolite (Ir_4/DAY zeolite). Dark-blue bars refer to a 20 H_2:20 D_2: 60 He reaction mixture, and the light-blue ones refer to a 20 H_2:20 D_2:40 He:20 C_2H_4 reaction mixture (mol ratios).

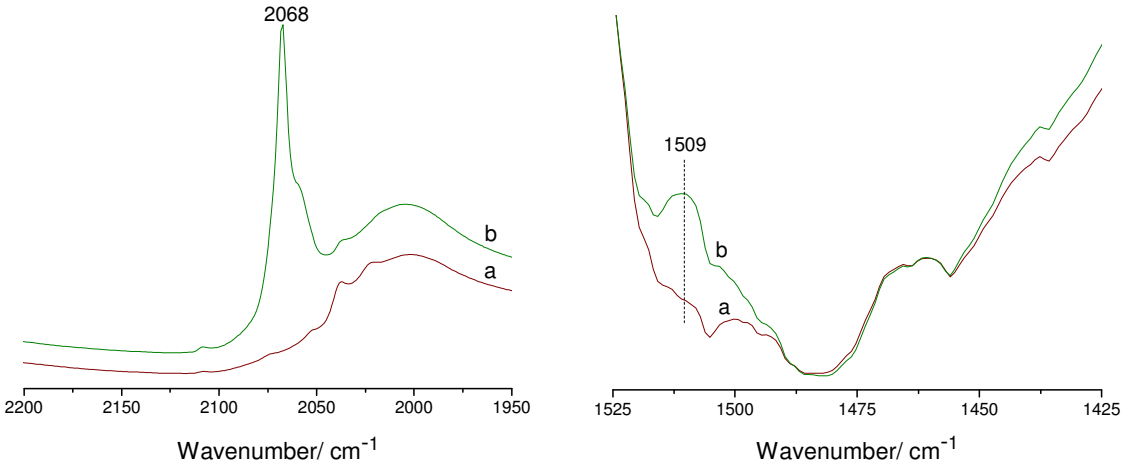

Figure S23. IR spectra characterizing the catalysts formed by deposition of $Ir(C_2H_4)_2$ species on the surface of zeolite DAY under the following flow conditions: a) He flow at 298 K and 1 bar, and b) H_2 (left) or D_2 (right) flow at 298 K and 1 bar.

1. Uzun, A.; Gates, B. C. *Angew. Chem. Int. Ed.*. **2008**, *47*, 9245.
2. Uzun, A.; Bhirud, V. A.; Kletnieks, P. W.; Haw, J. F.; Gates, B. C. *J. Phys. Chem. C* **2007**, *111*, 15064.
3. Uzun, A.; Ortalan, V.; Browning, N. D.; Gates, B. C. *J. Catal.* **2010**, *269*, 318.
4. Niu, H.; Yang, Q.; Tang, K.; Xie, Y. *Micropor. Mesopor. Mater.* **2006**, *96*, 428.
5. Bhirud, V. A.; Uzun, A.; Kletnieks, P. W.; Craciun, R.; Haw, J. M.; Dixon, D. A.; Olmstead, M. M.; Gates, B. C. *J. Organomet Chem.* **2007**, *692*, 2107.
6. Okamoto N. L.; Reed B. W.; Mehraeen S.; Kulkarni A.; Morgan D. G.; Gates B. C.; Browning N. D. *J. Phys. Chem.C* **2008**, *112*, 1759.
7. Jentoft, R. E.; Deutsch, S. E.; Gates, B. C. *Rev. Sci. Instrum.***1996**, *67*, 2111.